Jacob, L., and M. Tangstad. 2026. Temperature dependence of SiO formation in hydrogen atmosphere. In *Silicon for the Chemical and Solar Industry XVIII,* edited by M. Tangstad, H. Rong, A. Valderhaug, B. Andresen, H. Dalaker, and I. G. Page. Kristiansand, Norway, September 7–10. https://doi.org/10.55669/oa900829

Temperature dependence of SiO formation in hydrogen atmosphere

Liya Jacob[1*] and Merete Tangstad[1]

[1*] Department of Materials Science and Engineering, Norwegian University of Science and Technology, 7491, Trondheim, Norway

*Corresponding author: Liya Jacob, Email: liyamol.jacob@ntnu.no

Keywords: SiO formation, SiO reduction, Hydrogen based reduction, Kinetics

Abstract – The $Si + SiO_2 \rightarrow 2SiO$ reaction was investigated under carbon free conditions in hydrogen and argon atmospheres at 1600–1700 °C to quantify the activation energy and understand how gas environment influences SiO formation. Isothermal mass loss data were evaluated using a diffusion model, which showed linearity across all temperatures (R^2 = 0.92–0.99), suggesting diffusion through a growing SiO_x interfacial layer as the rate controlling step. Arrhenius analysis yielded activation energies (Ea) of 740 kJ·mol^{-1} in Ar and 582 kJ·mol^{-1} in H_2, and the values are consistent with transport limited Si–SiO_2 systems. The high Ea for both argon and hydrogen system also reveals that the reaction on the reactant surface also play an important role in the kinetics along with diffusion. The higher Ea in argon arises from the strongly suppressed SiO formation at 1600 °C, which steepens the temperature dependency. EPMA revealed coarse, sparse Si precipitates in Ar at 1600 °C, whereas hydrogen produced fine, uniformly dispersed Si domains, indicating earlier onset of defect formation and SiO transport. Condensation behaviour followed the amount of SiO formed.

1. INTRODUCTION

Hydrogen is increasingly viewed as a key enabler for carbon-neutral metallurgy because it can replace carbon-based reductants and support process routes that avoid fossil CO_2 emissions. The SiH2 (Ringdalen et al., 2024) concept highlights that future silicon production may rely on hydrogen-based routes. Realizing such a process requires conditions where SiO gas is generated, transported and reduced without rapid back-reaction to Si and SiO_2. The SiH2 investigations show that SiO behaviour is governed by slow and temperature-dependent kinetics, and that suppression of SiO condensation is a central challenge. These findings create a need for fundamental kinetic data for the $Si + SiO_2 \rightarrow 2SiO$ reaction in carbon-free atmospheres, including how hydrogen and argon influence defect formation, interfacial transport and SiO stability.

Although $Si + SiO_2 \rightarrow 2SiO$ reaction has been widely examined in carbon-containing systems, where SiO subsequently reacts with carbonaceous species, its intrinsic kinetics under carbon-free conditions remain poorly understood(Bao et al., 2013). Reported activation energies for SiO-forming reactions span a broad range—from ~380 kJ·mol^{-1} in thin-film geometries to 438–528 kJ mol^{-1} in powders and briquettes, and up to ~557 kJ·mol^{-1} in compacted beds(Sindland and Tangstad, 2021, Andersen, 2010, Leroy et al., 2020). The rate is dependent on microstructure, porosity, and mass-transport. These variations underscore that the apparent activation energy (Ea) is shaped not only by the chemical step but also by diffusion through the evolving SiO_x ($1<x<2$) interfacial layer and by gas-phase transport of SiO away from the reaction front (Li et al., 2016).

Recent studies have shown that hydrogen further modifies these processes by enhancing oxygen-vacancy formation, increasing defect mobility in SiO_2, and accelerating gas-phase transport (Cartier et al., 1993). Hydrogen has been observed to increase the rate of SiO formation, alter the morphology of condensed Si/SiO_2 products, and thin the gas-boundary layer relative to inert atmospheres. However, despite these mechanistic insights, no systematic determination of the activation energy of the $Si + SiO_2 \rightarrow 2SiO$ reaction has been performed under hydrogen and argon in a carbon-free environment.

In this work, we quantify the activation energy of the $Si + SiO_2 \rightarrow 2SiO$ reaction in hydrogen and argon atmospheres using isothermal kinetic data collected between 1600 and 1690 °C under carbon-free conditions. This will be done by extracting temperature-dependent rate constants from kinetic formulations and construct Arrhenius relationships for each atmosphere. This study will provide direct comparison of the activation energy in H_2 and Ar for SiO formation, offering new insight into how gas atmosphere and temperature affect Si–O kinetics.

2. MATERIALS AND METHODS

Experiments were carried out in an ENTECH 1800 resistance furnace equipped with tungsten carbide (WC) heating elements and capable of reaching 1700 °C. To ensure a fully carbon-free environment and prevent the thermodynamically favorable reaction between SiO and carbon (Bootsma et al., 1971), the hot zone was constructed entirely from alumina components, alumina tubes and Alsint 99.7 crucibles. Temperature control was achieved using a Eurotherm 2408 regulator connected to a custom LabVIEW interface, which continuously logged wall and crucible temperatures as well as furnace power through a National Instruments thermocouple acquisition system. Temperatures were monitored both at the crucible center and along the inner wall. Representative figure of the furnace is given in Figure 1.

16

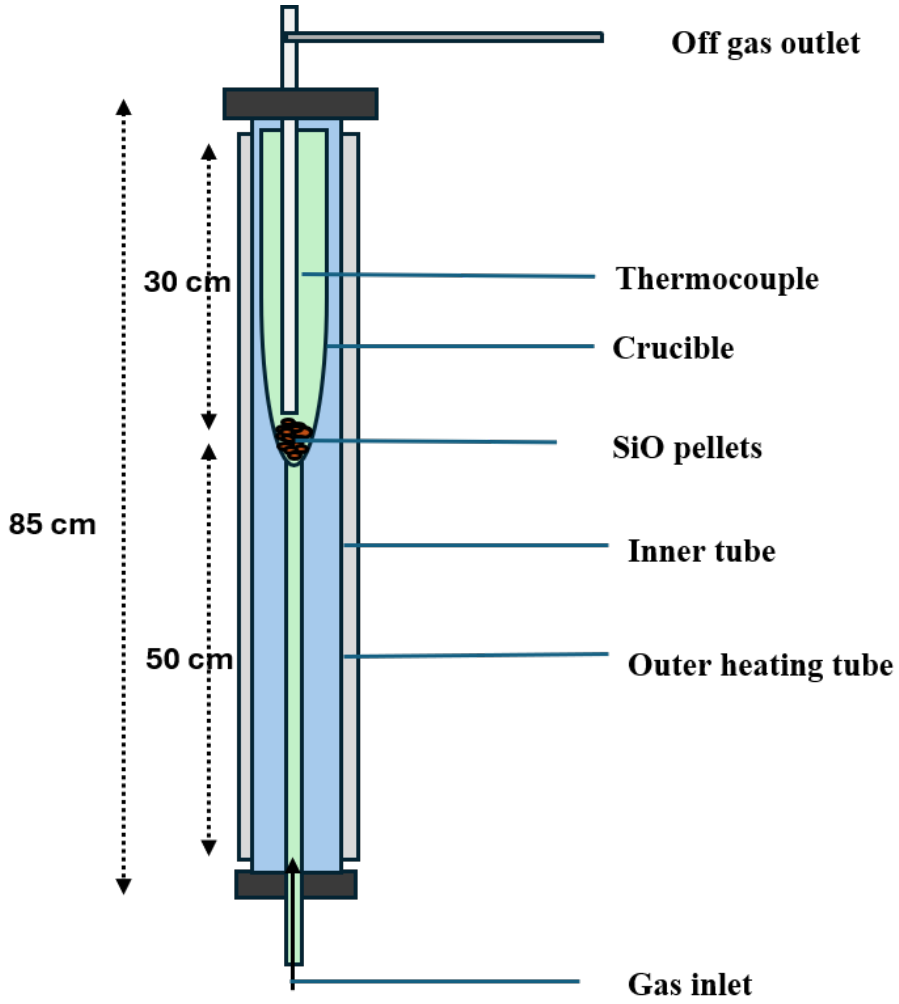

Figure 1. ENTECH 1800 alumina tube furnace used for the SiO formation experiments.

An alumina crucible was positioned at the furnace centre such that its base coincided with the hottest zone. This is where SiO generation takes place. Process gases (Ar or H_2) entered the crucible from below. The crucible remained open to allow off-gas release and to accommodate thermocouple insertion. A small alumina sieve was placed at the bottom of the crucible, and for each experiment, 10 g of SiO granules were distributed in a single layer on the sieve to maintain open gas flow through the bed. The furnace was heated at 10 °C min^{-1} to 1700 ,1650, 1600 °C and held such that the lower crucible region remained at the set temperature for a period of 5, 30, 60 and 90 mins. Argon was supplied at 0.25 L·min^{-1} during heating, while hydrogen was introduced once the temperature reached the set temperature. After cooling down to below 50 °C, the crucible was removed and the products were collected. The crucible was weighed before and after each experiment, and all recovered material, both from the sieve and from the crucible walls, was classified into unreacted pellets and various condensates of different morphologies ("flowers," "plates," and "dust").

Silicon monoxide was supplied as Patinal "SiO" granules (Merck; CAS 10097-28-6) with an Si/O ratio of 1. The granules, 3–5 mm in size (Figure 2), were confirmed by SEM and EPMA to be dense, homogeneous, and free of visible porosity or distinct Si/SiO_2 phase boundaries. High-purity argon (99.9%, Instrument Ar 5) and hydrogen (99.9%, Instrument H_2 4.5) were provided by Linde. The figure of the crucible, and the samples can be seen in our previous publications(Liya Jacob, 2026b, Liya Jacob, 2026a).

2.1. Activation-Energy Determination

The activation energy was obtained from isothermal mass-loss data using a one-dimensional diffusion model D1 (Bieniasz, 2015). Even though, we used a diffusion model, it was the best mechanistic fit rather than a reaction controlled by diffusion alone. Conversion was calculated as,

$$\alpha(t) = \frac{m_0 - m(t)}{m_0},$$

and the rate is given by,

$$\frac{d\alpha}{dt} = \frac{k}{2\alpha}$$

was evaluated for each time point. For each isothermal experiment at 1700, 1650 and 1600 °C, $g(\alpha) = \alpha^2$ was plotted against time and the apparent rate constant $k(T)$ was taken as the slope of a linear least-squares fit to the early-to-mid conversion region, where diffusion control is dominant. The activation energy was found based on the Arrhenius equation:

$$k = k^0 \exp\left(\frac{-E_a}{RT}\right)$$

where k is the experimentally derived rate constant, k^0 is the pre-exponential factor, E_a is the activation energy, R is the gas constant ($R = 8.314\ J \cdot mol^{-1} \cdot K^{-1}$), and T is the absolute temperature in Kelvin. Uncertainty in E_a was estimated from the standard error of the regression slope.

3. RESULTS AND DISCUSSION

The D1 model was chosen because the conversion data showed the typical concave-down behaviour and steady rate decrease. Even though, this method is generally used in diffusion controlled systems, our choice was rather because of good mechanical fit rather than the rate being purely governed by diffusion. When the D1 integral form $g(\alpha) = \alpha^2$ was fitted to the isothermal data, the linear regressions produced R^2 values of 0.92–0.99 both in Ar and H_2 at all three temperatures. Morphological evidence from our earlier publication supports this choice (Liya Jacob, 2026b, Liya Jacob, 2026a). The kinetic profiles at 1700, 1650, and 1600 °C show a consistent enhancement of the $Si + SiO_2 \rightarrow 2SiO$ reaction in hydrogen compared with argon.

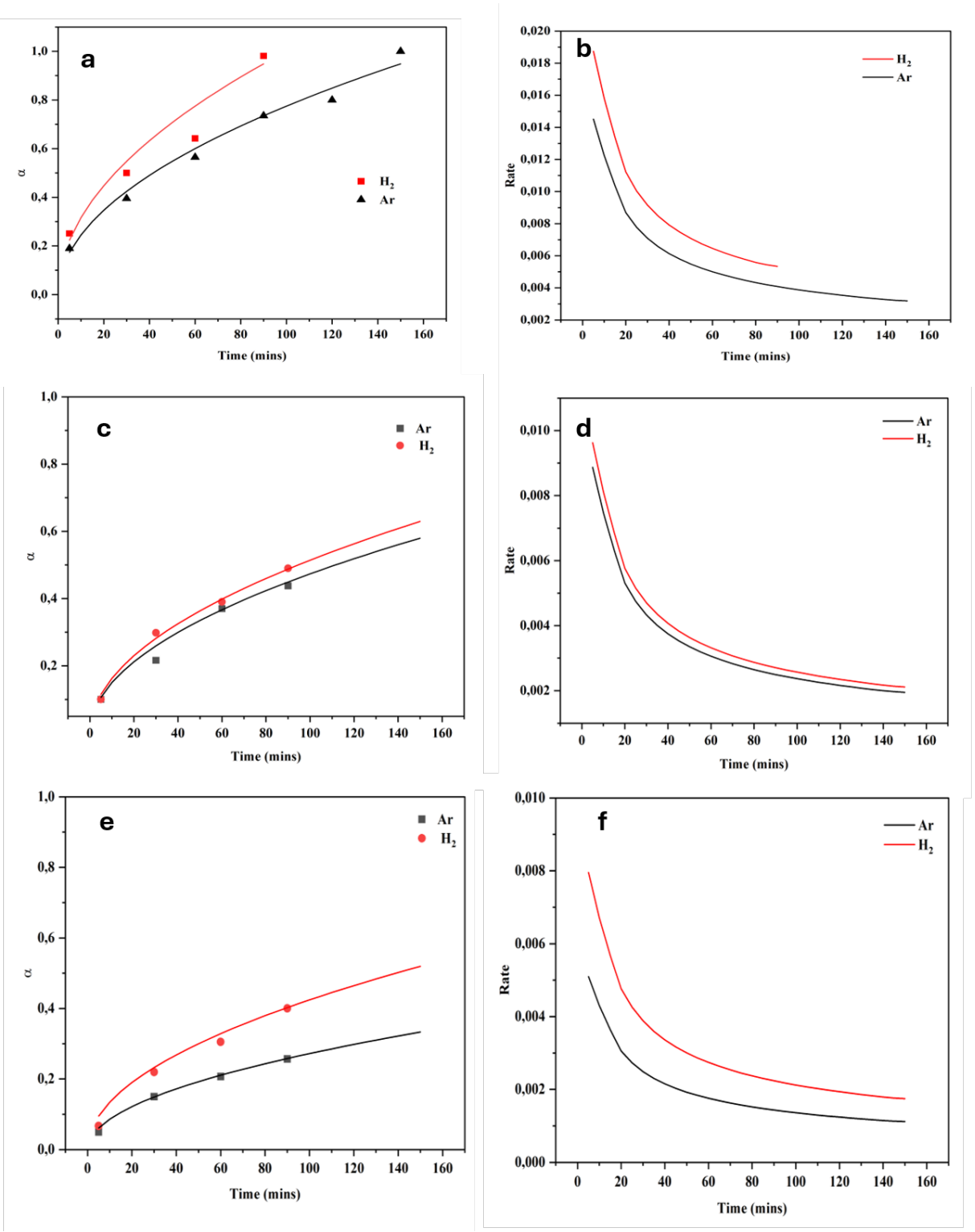

Figure 2. Rate and conversion profile of SiO formation in argon and hydrogen at 1700 °C (a-b), 1650 °C (c-d), 1600 °C (e-f).

In all α–time curves, hydrogen reaches higher conversion at each temperature, and the separation between the two atmospheres becomes more pronounced as temperature decreases. The rate–time plots show the expected decline in reaction rate as the interfacial SiO_x layer thickens, and the rate–α relationships confirm that hydrogen maintains a higher instantaneous rate at equivalent conversion. The Arrhenius analysis yields activation energies 740 $kJ \cdot mol^{-1}$ in Ar and 582 $kJ \cdot mol^{-1}$ in H_2. The Arrhenius fit for hydrogen looks poor because

the three hydrogen rate constants do not fall on a clean straight line, which means the reaction in hydrogen does not follow a single, simple Arrhenius behavior across the temperatures. In hydrogen, the mechanism might change slightly with temperature. Defect formation, surface roughening and SiO transport all increase, so the effective rate constant is influenced by more than just the activation barrier. As a result, the hydrogen points shift up or down relative to the ideal line, giving a weaker linear trend and a lower R^2. Argon behaves more simply and stays closer to a single mechanism, so its points align better.

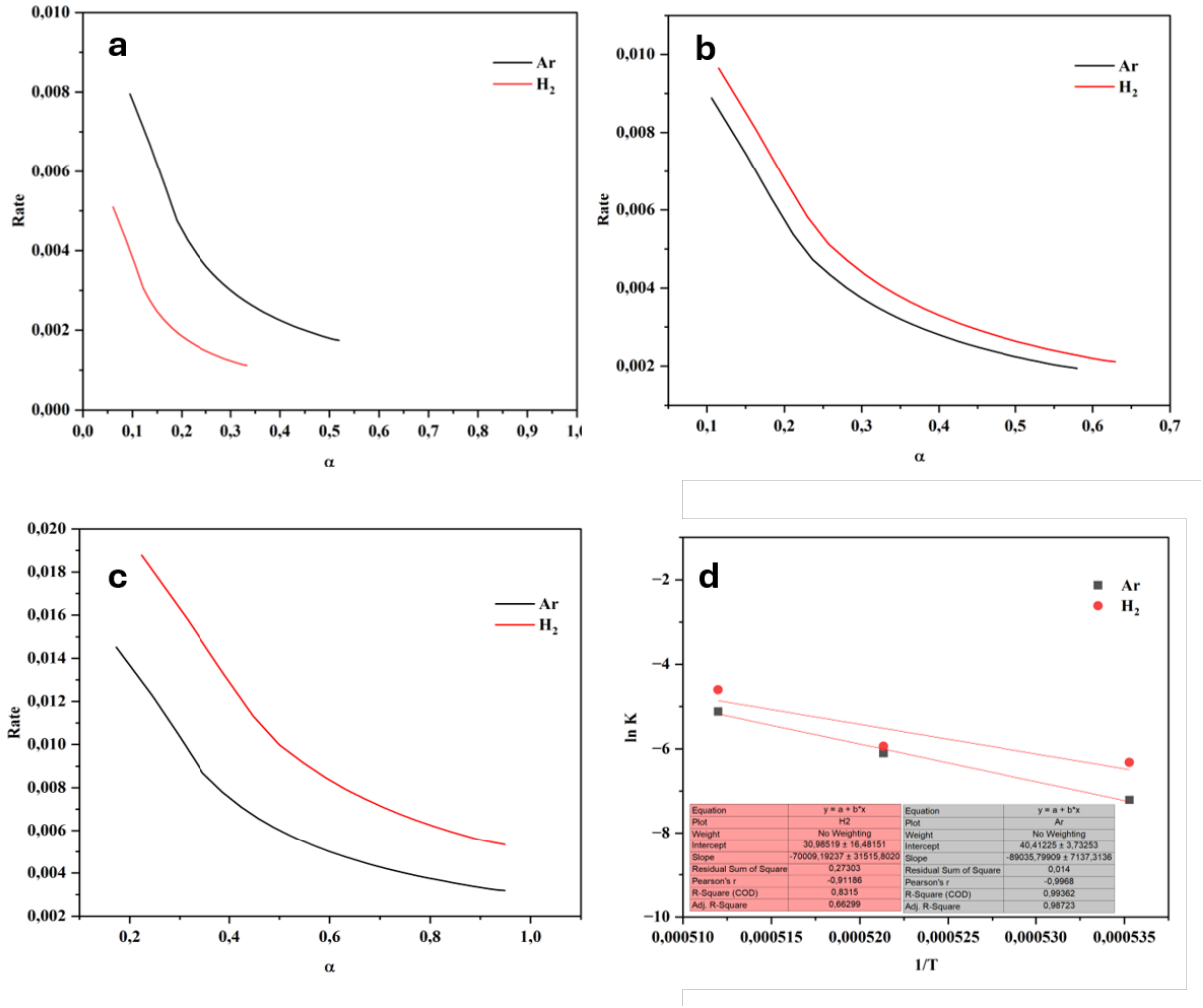

Figure 3. Rate and conversion profiles for a: 1600, b: 1650 and c: 1700 °C. d: Arrehnius plot.

Raider (Raider, 1988) described the formation of sub stoichiometric layers during SiO generation, and Devine et al. (Devine et al., 1996, Devine et al., 1993) demonstrated that oxygen vacancy formation and SiO out diffusion occur readily in SiO_2 at high temperature. Ozturk and Fruehan (Ozturk and Fruehan, 1985) identified gas phase mass transfer as a controlling factor in silica reduction by hydrogen at 1650 °C, and Han and Sohn (Han and Sohn, 2005) reported similar behavior at 1285–1450 °C. The present data follow these trends: at 1700 °C the difference between the two gases is moderate, but at 1650 and 1600 °C hydrogen maintains significantly higher rates and reaches higher conversion within the same reaction time. The overall behavior is consistent with literature showing that apparent activation energies for SiO forming reactions increase with diffusion path length and gas phase resistance (Bongiorno and Pasquarello, 2004, Devine et al., 1996), with powders and briquettes of SiO (Si-SiO_2 interfaces) typically yielding higher values than thin films. The stronger enhancement in hydrogen at

lower temperatures indicates that the effective transport barrier is reduced relative to argon, which agrees with the higher diffusivity and stronger chemical interaction of hydrogen with the SiO_2 network (Watanabe, 2025).

The Arrhenius analysis yields activation energies 740 $kJ \cdot mol^{-1}$ in Ar and 582 $kJ \cdot mol^{-1}$ in H_2, which are high but still consistent with the upper range reported for compact or diffusion limited Si–SiO_2 systems. Powder and briquette studies of Si + SiO_2 → 2SiO typically report apparent activation energies between about 438-528 $kJ \cdot mol^{-1}$ (Andersen, 2010), and ~557 $kJ \cdot mol^{-1}$ (Sindland and Tangstad, 2021) have been obtained for densely packed beds where long solid state and gas phase diffusion paths dominate the overall resistance. In contrast, thin film geometries, where SiO can escape over nanometer scale distances, give significantly lower barriers around 4.0 eV (≈386 $kJ \cdot mol^{-1}$), and the disproportionation of solid SiO to Si + SiO_2 has been assigned an activation energy of only about 82 $kJ \cdot mol^{-1}$, reflecting a much shorter transport length and a different rate controlling step (Leroy et al., 2020).

The higher activation energy in Ar compared with H_2 is consistent with the lower gas phase diffusivity of Ar. CO was used as a surrogate for SiO to calculate the diffusivity of H_2 and Ar in SiO, and at 1673 °C, they typically have values of 1.73×10^{-3} m^2/s in H_2 and 4.55×10^{-4} m^2/s in Ar (Liya Jacob, 2026b). Hydrogen is known to enhance oxygen vacancy formation and defect mobility in SiO_2, to promote Si–H and Si–OH species, and to increase gas phase mass transfer, all of which reduce the effective transport barrier for SiO escape and thus lower the apparent activation energy relative to Ar (Luo et al., 2026, Rashkeev et al., 2001, Bunson et al., 2000, Alkauskas and Pasquarello, 2007). In this context, the value of about 582 $kJ \cdot mol^{-1}$ in H_2 can be viewed as a transport limited activation energy characteristic of a thick, defect rich SiO_x layer under hydrogen.

In addition, as the pellet reacts, its surface becomes rougher, fragmented, and more porous and the pellet becomes smaller. This means the effective reaction area decreases with time**,** so the measured rate constant is not purely intrinsic. It also reflects evolving geometry. In diffusion-controlled systems, the flux of SiO depends on the thickness of the SiO_2 and Si layer, the local porosity and microcracks and the changing surface area**.** When the pellet breaks into smaller pieces or develops pores, or become smaller due to the reaction proceeding, the contact area between Si and SiO_2 increases, which decreases the instantaneous rate even if the intrinsic diffusion coefficient is unchanged. This produces curvature in α–t and rate–t plots and can inflate the apparent activation energy because the Arrhenius fit assumes a constant geometry. Figure 4 shows the proposed mechanism of the reaction. This effect is well-documented in solid–solid reactions where reaction progress changes the interface area, causing deviations from ideal shrinking-core or planar-interface kinetics. Sindland et al. (Sindland and Tangstad, 2021) used the change in contact area for determining the rate of SiO formation.

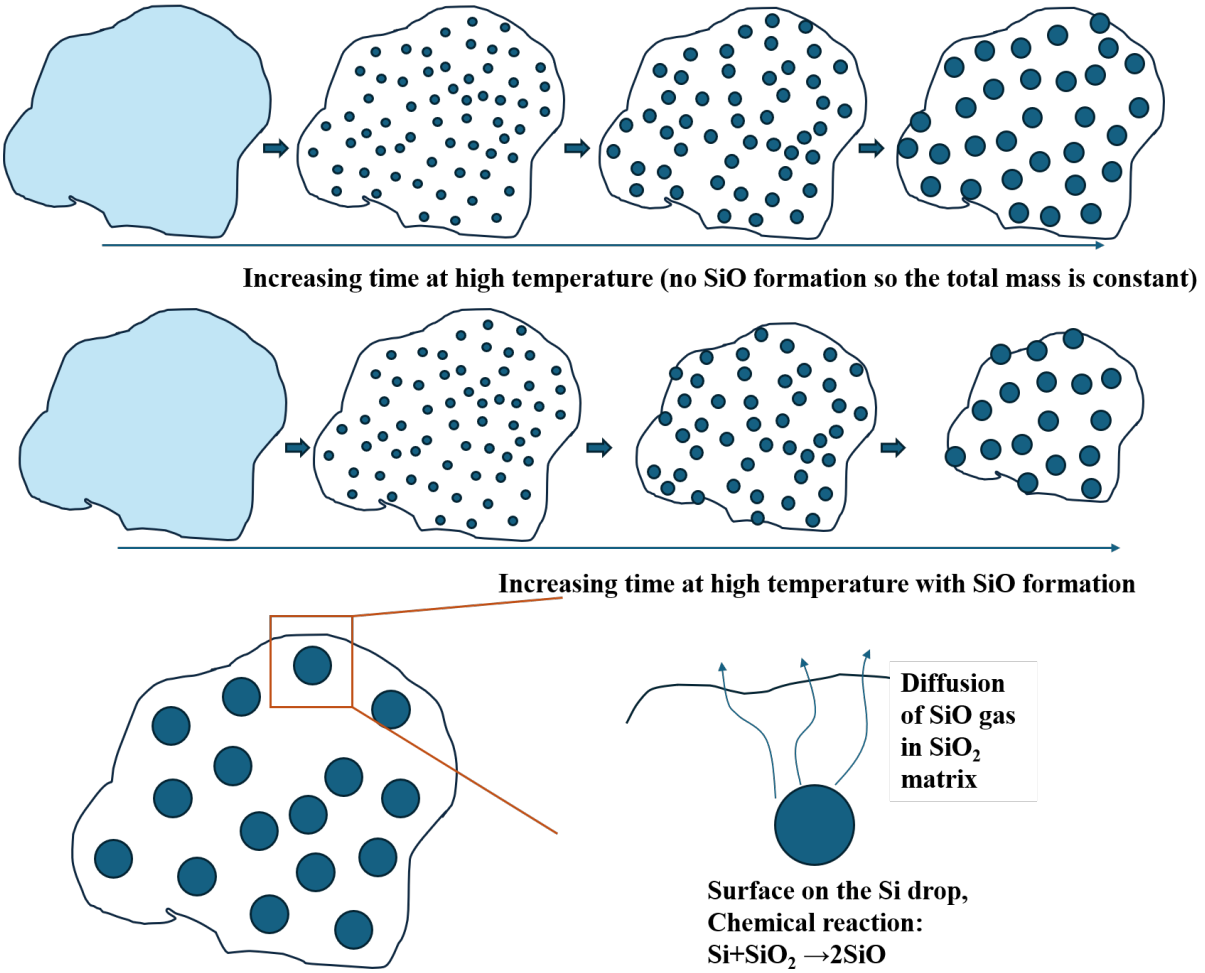

Figure 4. The proposed mechanism of the formation of Si and SiO_2 islands and the diffusion through the interphase.

Bongiorno et al. (Bongiorno and Pasquarello, 2004) studied the transport of O_2 through SiO_2 at Si-SiO_2 interphase using oxidation reactions at different diffusion lengths. They show that the effective diffusion length through a SiO_2 layer is set by the macroscopic diffusivity D of the mobile species and the experimental time scale via the relation $L_D = (4Dt)^{1/2}$. Because D is determined by a broad distribution of local hopping barriers in the disordered oxide, any increase in local barrier heights or reduction in site connectivity produces a strong reduction in D and therefore a rapid shortening of L_D. A thin, higher-density interfacial oxide adjacent to Si acts as a low-permeability layer. It reduces the number of percolating low-energy pathways, lowers the effective D relative to bulk SiO_2 and confines transport when the oxide thickness becomes comparable to or larger than L_D. Because D follows an Arrhenius law, $D \propto \exp(-E_D/RT)$, the diffusion length inherits an exponential temperature sensitivity ($L_D \propto \exp(-E_D/2RT)$), so modest changes in the activation energy for diffusion produce large changes in L_D at the temperatures used here. For our experiments, this provides a consistent explanation of the observed transport limitation and large apparent activation energies. A dense interfacial SiO_x layer and poor percolation in Ar reduce D and L_D, suppressing SiO escape at lower temperatures, whereas hydrogen modifies the local structure and lowers effective barriers, increases D and extends L_D, thereby enhancing SiO flux and lowering the apparent activation energy. Ogawa and Shiono (Ogawa and Shiono, 1995) studied the effect of hydrogen on the interface. They showed that the hydrogen strongly controls reactions at the Si–SiO_2 interface by both creating and removing electrically active defects and by moving through the oxide. From this microscopic understanding of the interface defects, the low-field

instability is closely related to the dissociation chemistry (the reverse of passivation) of hydrogen from hydrogen-passivated dangling Si bonds. The rate at which the reaction causing the generation of interface traps takes place is controlled by the diffusion of hydrogen that has been released from hydrogen-passivated defect sites previously. In plain terms, hydrogen can speed up or slow down interface reactions depending on how easily hydrogen atoms or molecules can move away from the interface. If hydrogen diffuses away quickly the interface becomes more reactive because passivating hydrogen is removed, while slow hydrogen transport lets released hydrogen re-passivate sites and suppress defect growth.

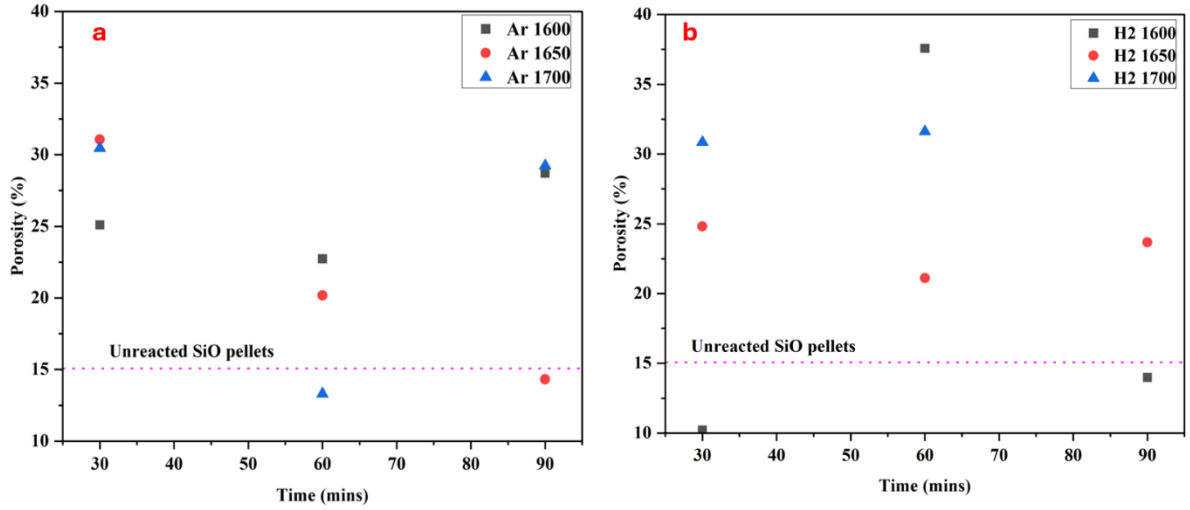

Figure 5. Porosity of the pellets across different temperatures and time.

Porosity measurements as shown in Figure 5 show large scatter because different pellets from the same batch already have different initial porosity and appearance. To reduce this effect, three pellets were selected for each condition and averaged. Even with this variation, the data clearly indicates that porosity can become almost twice that of the unreacted pellets as temperature and reaction time increase, reflecting the progressive opening and fragmentation of the structure. As the reaction approaches completion around 90 minutes, some pores may collapse and merge into thicker, more compact regions, which can reduce the measured porosity and further complicate the trend. Overall, hydrogen tends to give slightly higher porosity values than argon at comparable conditions, but a strict conclusion cannot be drawn because of the pellet-to-pellet variation and the dynamic changes in pore formation and collapse during the reaction.

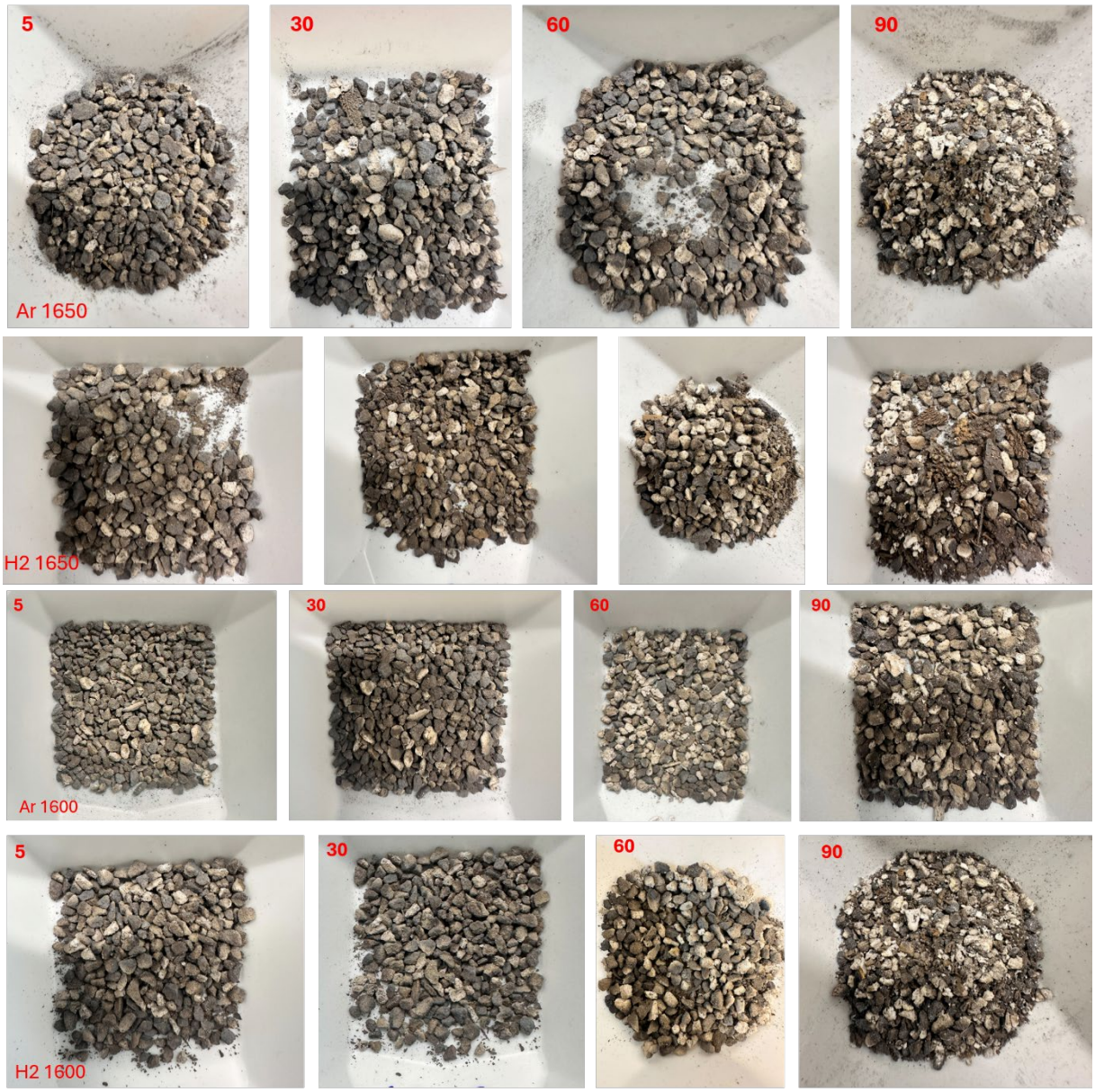

Figure 6. Visual appearance of pellets at different temperatures.

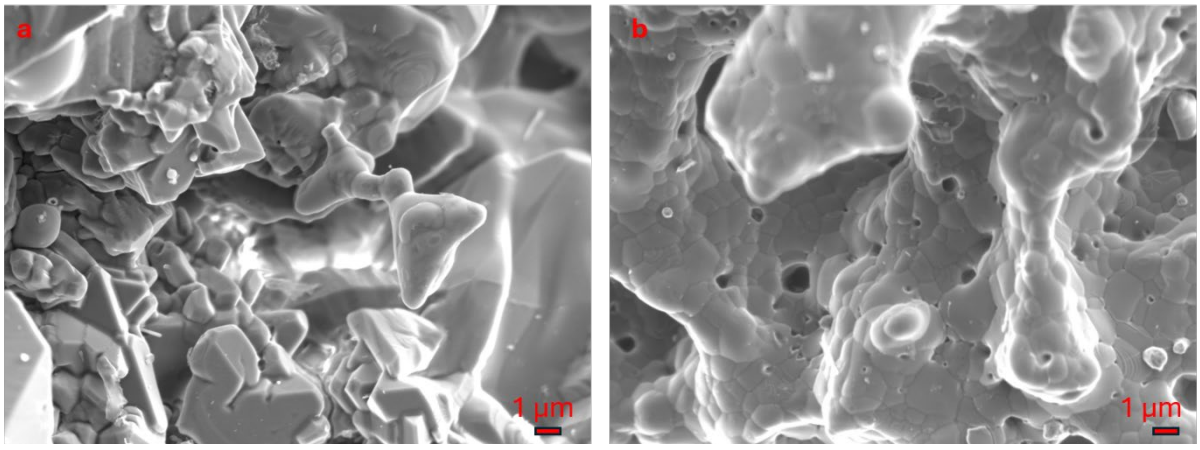

Figure 7. SEM image of the pellets after 30 minutes of experiment in 1700 °C. a: Ar and b: H_2.

Figure 6 and Figure 7 show that the pellets treated in hydrogen develop a noticeably more open and irregular surface, with small voids, pits, and shallow pores scattered across the

grains, while the pellets treated in argon remain much more compact and faceted. This difference does not indicate a fully developed pore network, but it does show that hydrogen slightly roughens and disrupts the SiO_2/Si surface during reaction. Hydrogen promotes local reduction and vacancy formation, so small pockets form where material has been removed or rearranged as SiO leaves the solid. In argon, vacancy formation is weaker and the surface stays dense, so the grains retain their sharp, angular morphology. Overall, hydrogen produces a subtly more porous and irregular microstructure, whereas argon preserves a smoother, more compact surface, even though neither atmosphere creates a continuous pore network.

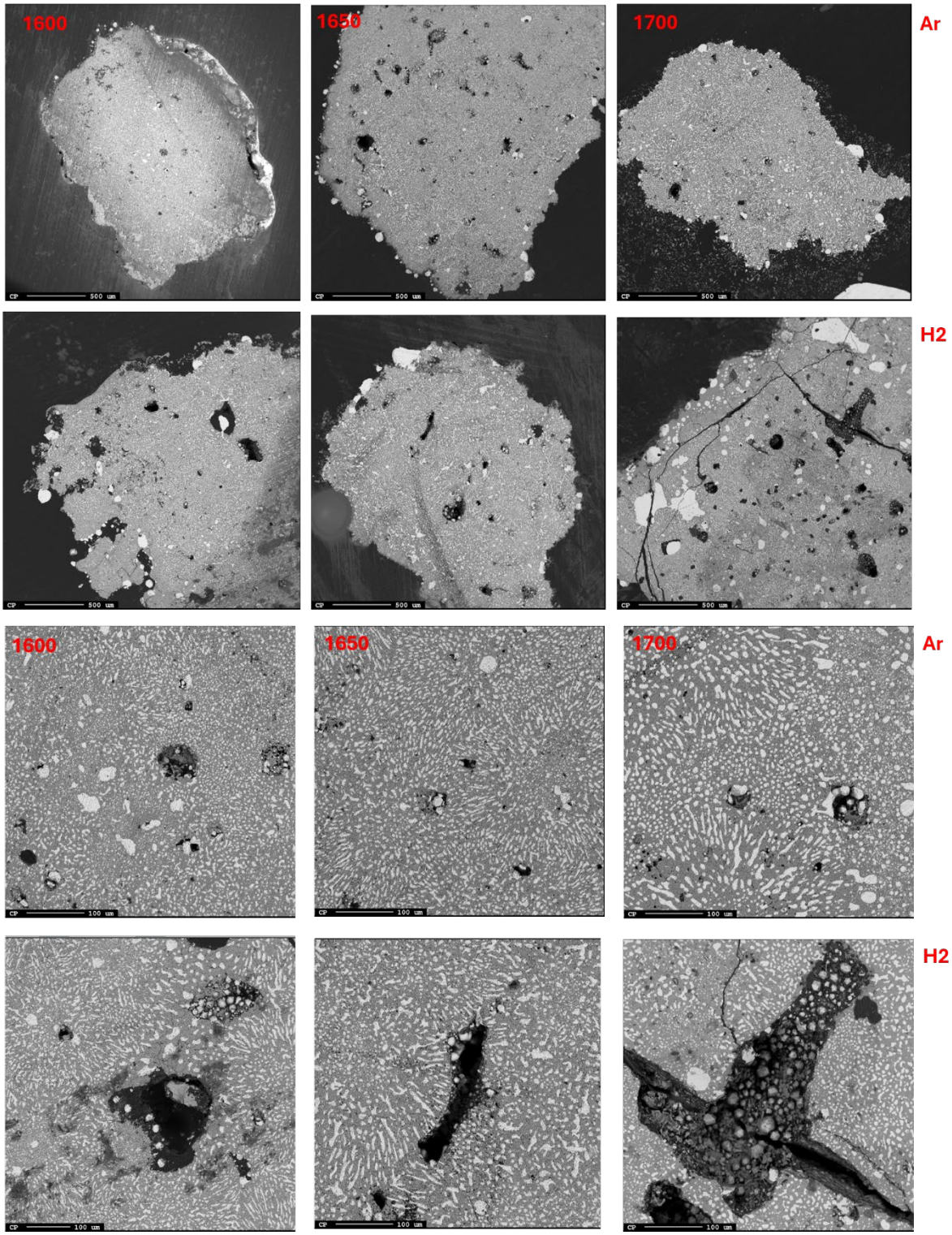

Figure 8. Back-scattered electron-EPMA analysis of the pellets at 500 µmb(200x) and 100 (40x) µm.

Figure 8 shows the back-scattered EPMA cross-sections reveal a clear temperature-dependent transformation of the SiO granules. At 1600 °C, pellets reacted in Ar show coarse, irregular Si precipitates embedded within a largely continuous SiO_2 matrix, indicating limited SiO transport and slow development of the oxygen-depleted interfacial layer. In H_2 at the same temperature, the Si domains are finer and more uniformly dispersed. At 1650 °C, the Ar samples display Si coarsening and the emergence of elongated Si regions, consistent with

slower evacuation of SiO and stronger local disproportionation. The appearance of pores where the formation of Si crystals start also is higher in H_2 pellets.

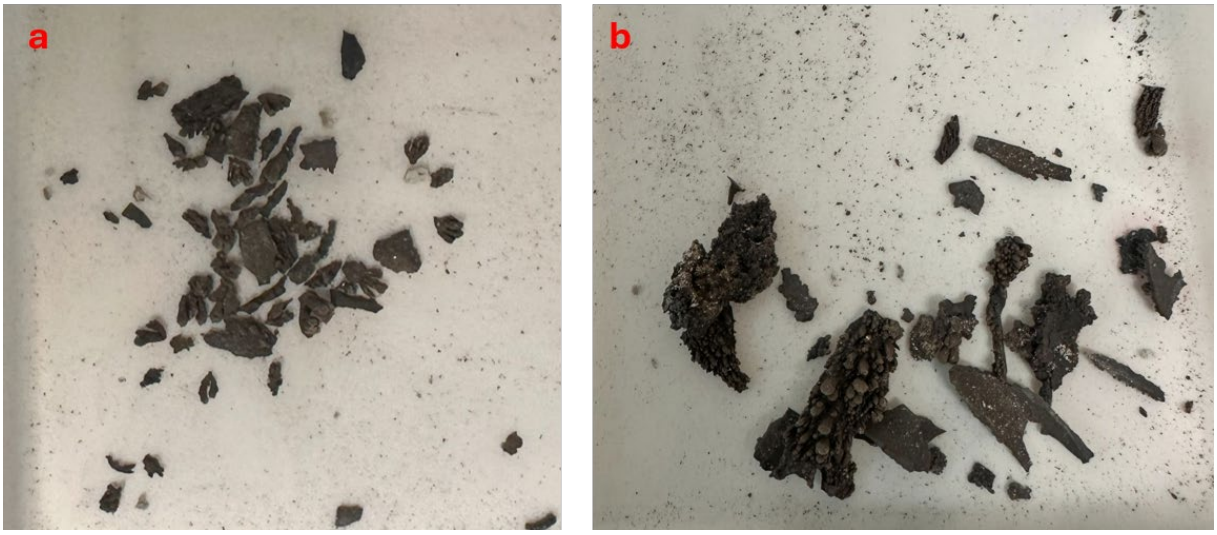

Figure 9. The flower morphology of the condensate in a: Ar and b: H_2

After the SiO is formed, it will be transformed back to $Si+SiO_2$ on the colder crucible walls, and some will fall into the crucible bottom. The flower shaped condensates, found on the crucible, are generally nucleated on the crucible wall, and fall when cooling. The two condensates shown in Figure 9 have a flower-like morphology. This forms in both atmospheres and reflects the way SiO vapor condenses rather than a strong gas-dependent effect. In argon (a), the condensate breaks into many small, brittle fragments with petal-like edges, while in hydrogen (b) the pieces are larger and more clustered, but the overall "flower" appearance is still present. This morphology develops because SiO vapor reaches supersaturation and solidifies in radiating, outward-growing clusters; once cooled and handled, these clusters fracture into petal-shaped pieces. The images therefore show that the fundamental condensation mechanism is the same in both gases, and the flower shape is a natural outcome of SiO vapor condensing and cracking, with only minor differences in size and compactness between argon and hydrogen.

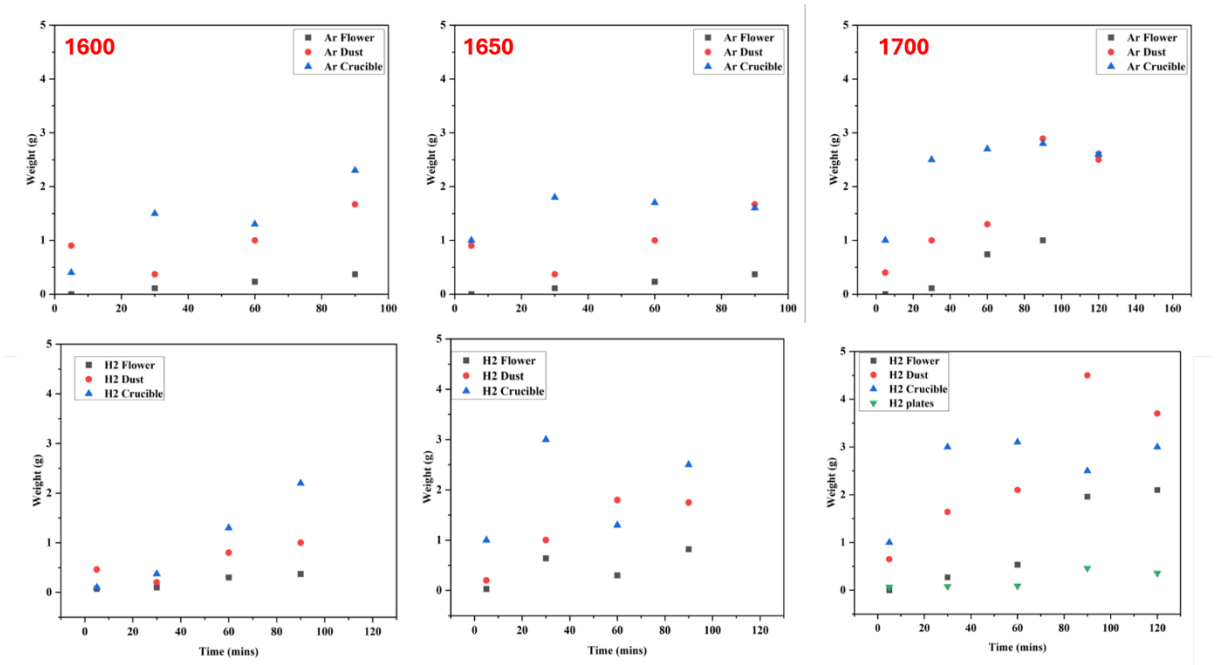

Figure 10. Condensate weight in gram.

The condensate collected are shown in Figure 10 broadly similar mass evolution, but the morphology of the recovered material varies with both atmosphere and temperature. In all cases the condensate separates into loose "flower" fragments, fine dust, and a crucible-bound fraction that solidifies directly on the crucible wall and cannot be removed without breaking it, indicating strong adhesion and high local supersaturation. At 1700 °C in hydrogen a distinct plate-like condensate appears, a morphology not observed at lower temperatures or in argon. This suggests that at the highest temperature hydrogen enables a different condensation pathway in which SiO vapor grows as broad, layered structures before fracturing, whereas argon maintains the typical petal-like clusters across all temperatures. The weight trends therefore reflect not only the amount of SiO leaving the pellets but also how the vapor condenses under each atmosphere, with hydrogen at 1700 °C producing a unique structural form while the overall condensate mass remains comparable.

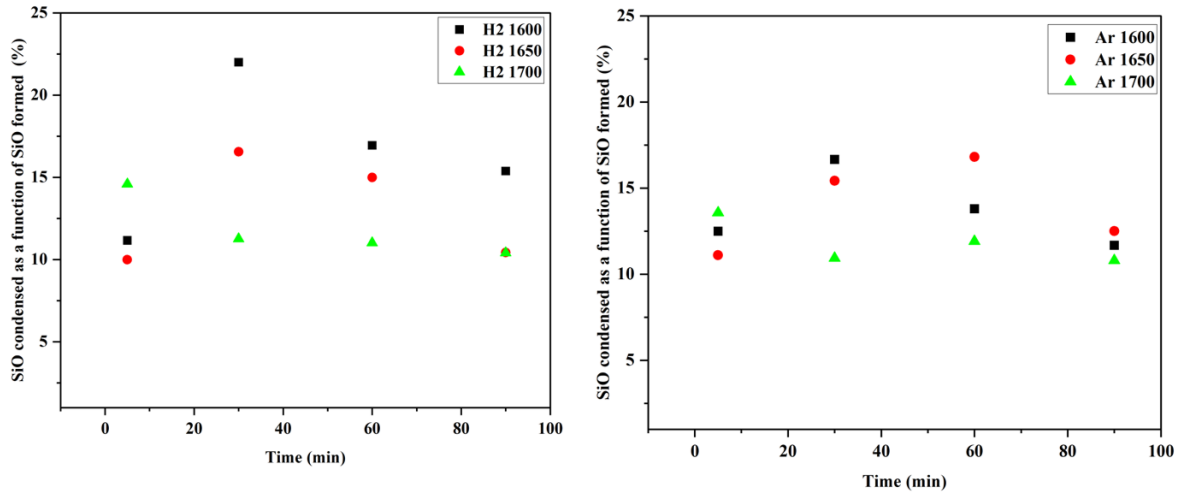

Figure 11. The percentage of SiO condensed at the crucible wall as a function of SiO formed in argon and hydrogen.

The percentage of SiO that condenses follows the amount of SiO formed, and the trend is similar in both argon and hydrogen. At all temperatures, the condensed fraction increases steadily as more SiO is produced, confirming that condensation is governed mainly by the SiO supply rate rather than by the gas atmosphere. Hydrogen shows a smoother, more gradual increase in condensed fraction, reflecting faster and more uniform SiO generation and transport. In argon, the condensed fraction shows stronger fluctuations at higher temperatures, which may be due to slower gas-phase transport and more local supersaturation, causing SiO to condense in larger, less uniform aggregates.

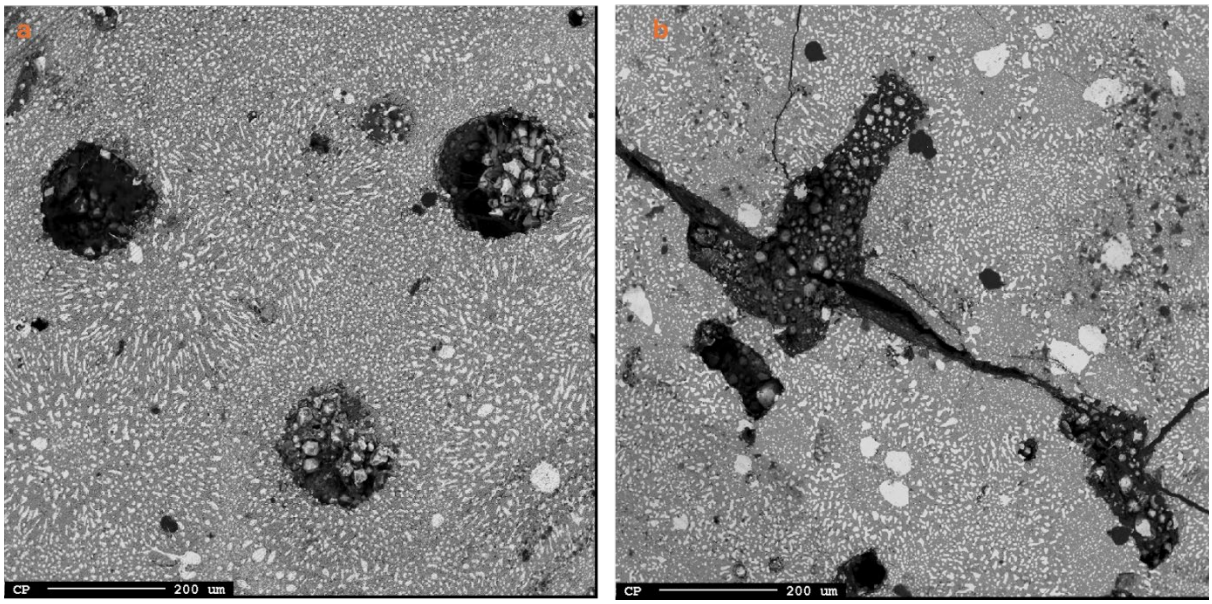

Figure 12. Si formation on the pores of a: argon and b: hydrogen and 1700 °C.

When silicon crystals nucleate and grow on pore surfaces as shown in Figure 12, the process is driven by local supersaturation and heterogeneous nucleation at energetically favorable sites. Pores and internal voids act as microtraps for vapor-phase SiO, increasing local partial pressure and residence time so that supersaturation is reached there before the surrounding flat surfaces. The pore walls and edges lower the critical nucleus size and reduce the surface-energy penalty for nucleation, so condensation begins preferentially inside or at the rim of pores. Once nuclei form, they grow by direct impingement of SiO and by coalescence, producing coarse, clustered grains that fill or rim the pore. This pore-centered growth also reduces the net SiO flux leaving the solid because some vapor is captured and condensed locally, which in turn affects mass-loss measurements and the apparent kinetics. Besides this, most of the condensates starts nucleating around the cooler parts of the crucible (Liya Jacob, 2026a).

4. CONCLUSIONS

This study provides a systematic determination of the activation energy for the $Si + SiO_2 \rightarrow 2SiO$ reaction under hydrogen and argon in a carbon-free environment. Overall, it is shown that SiO formation is faster in H_2 than in Ar at all temperatures. The D1 diffusion model described the kinetics across all temperature's values and EPMA shows progressive development of an oxygen depleted SiO_x interfacial layer. Hydrogen consistently accelerated SiO formation, yielding a lower activation energy (582 $kJ \cdot mol^{-1}$) than argon (740 $kJ \cdot mol^{-1}$). The higher Ea in argon reflects the very slow SiO formation at 1600 °C, where pellets remain largely unmodified and Si precipitation is limited. In contrast, hydrogen promotes early defect formation, finer Si dispersion, and faster SiO removal because of higher diffusion, maintaining measurable reaction rates even at lower temperatures. Condensation behavior is proportional

with SiO formation in both atmospheres. These findings clarify how gas atmosphere governs high-temperature Si–O kinetics and provide a foundation for designing carbon-free silicon processes with improved efficiency and reduced material losses.

5. ACKNOWLEDGEMENTS

This paper is published by the SiH2 project financed by the Research Council of Norway through grant 325464. They are acknowledged. The authors declare no competing interests.

6. REFERENCES

ALKAUSKAS, A. & PASQUARELLO, A. 2007. Alignment of hydrogen-related defect levels at the Si–SiO2 interface. *Physica B: Condensed Matter,* 401**,** 546–549.

ANDERSEN, V. 2010. Reaction mechanism and kinetics of the high temperature reactions in the silicon process. *Norwegian University of Science and Technology, Trondheim***,** 89.

BAO, S., TANGSTAD, M., TANG, K. & RINGDALEN, E. 2013. *Production of SiO Gas in The Silicon Process*.

BIENIASZ, L. K. 2015. Models Involving One-Dimensional Diffusion. *In:* BIENIASZ, L. K. (ed.) *Modelling Electroanalytical Experiments by the Integral Equation Method.* Berlin, Heidelberg: Springer Berlin Heidelberg.

BONGIORNO, A. & PASQUARELLO, A. 2004. Multiscale modeling of oxygen diffusion through the oxide during silicon oxidation. *Physical Review B,* 70**,** 195312.

BOOTSMA, G. A., KNIPPENBERG, W. F. & VERSPUI, G. 1971. Growth of SiC whiskers in the system SiO2-C-H2nucleated by iron. *Journal of Crystal Growth,* 11**,** 297–309.

BUNSON, P., DI VENTRA, M., PANTELIDES, S., FLEETWOOD, D. & SCHRIMPF, R. 2000. Hydrogen-related defects in irradiated SiO/sub 2. *IEEE Transactions on Nuclear Science,* 47**,** 2289–2296.

CARTIER, E., STATHIS, J. H. & BUCHANAN, D. A. 1993. Passivation and depassivation of silicon dangling bonds at the Si/SiO2 interface by atomic hydrogen. *Applied Physics Letters,* 63**,** 1510–1512.

DEVINE, R., MATHIOT, D., WARREN, W. & ASPAR, B. 1996. O interstitial generation and diffusion in high temperature annealed Si/SiO2/Si structures. *Journal of applied physics,* 79**,** 2302–2308.

DEVINE, R. A. B., MATHIOT, D., WARREN, W. L., FLEETWOOD, D. M. & ASPAR, B. 1993. Point defect generation during high temperature annealing of the Si-SiO2 interface. *Applied Physics Letters,* 63**,** 2926–2928.

HAN, G. & SOHN, H. Y. 2005. Kinetics of the Hydrogen Reduction of Silica Incorporating the Effect of Gas-Volume Change upon Reaction. *Journal of the American Ceramic Society,* 88**,** 882–888.

LEROY, F., LANDRU, D., CHEYNIS, F., KONONCHUK, O., MüLLER, P. & CURIOTTO, S. 2020. Kinetics and coupled dynamics of dewetting and chemical reaction in Si/SiO 2/Si system. *Journal of Materials Science,* 55**,** 16074–16082.

LI, X., ZHANG, G., TRONSTAD, R. & OSTROVSKI, O. 2016. Reduction of Quartz to Silicon Monoxide by Methane-Hydrogen Mixtures. *Metallurgical and Materials Transactions B,* 47**,** 2197–2204.

LIYA JACOB, M. K., MERETE TANGSTAD. Silicon Production with Hydrogen as a Reductant: Towards Greener Ferrosilicon. COM 2026, 2026a Canada. Springer.

LIYA JACOB, M. K., MERETE TANGSTAD 2026b. SiO -formation and -condensation with hydrogen in carbon free conditions. *Submitted*.

LUO, H., QI, D., MA, Z., GUO, X., ZHOU, H., LIU, Y. & ZUO, X. 2026. First-principles study of hydrogen-related defects at the a-SiO2/Si(100) interface. *Scientific Reports,* 16**,** 17465.

OGAWA, S. & SHIONO, N. 1995. Generalized diffusion-reaction model for the low-field charge-buildup instability at the Si-SiO 2 interface. *Physical Review B,* 51**,** 4218.
OZTURK, B. & FRUEHAN, R. 1985. The rate of formation of SiO by the reaction of CO or H2 with silica and silicate slags. *Metallurgical Transactions B,* 16**,** 801–806.
RAIDER, S. I. 1988. The Role of SiO in Si Oxidation at a Si-SiO2 Interface. *In:* HELMS, C. R. & DEAL, B. E. (eds.) *The Physics and Chemistry of SiO2 and the Si-SiO2 Interface.* Boston, MA: Springer US.
RASHKEEV, S., FLEETWOOD, D., SCHRIMPF, R. & PANTELIDES, S. 2001. Defect generation by hydrogen at the Si-SiO 2 interface. *Physical review letters,* 87**,** 165506.
RINGDALEN, E., SVENUM, I.-H. & AARNæS, T. 2024. SiH2-A new process for Si-production based on hydrogen. *Available at SSRN 4942625*.
SINDLAND, C. & TANGSTAD, M. 2021. Production rate of SiO gas from industrial quartz and silicon. *Metallurgical and Materials Transactions B,* 52**,** 1755–1771.
WATANABE, T. 2025. Kinetics of thermal oxidation of silicon. *Applied Physics Express,* 18**,** 120101.

Liya Jacob

PhD, NTNU, Norway

Liya Jacob is a PhD researcher in Materials Science and Engineering at NTNU, specializing in hydrogen-based and plasma-assisted reduction pathways for sustainable metallurgical silicon production. Her doctoral work focuses on high-temperature reaction kinetics, sustainable metal production in hydrogen. She maintains strong professional interests in clean-energy process development, advanced furnace technologies, and low-emission materials production.
